

Characterising HOD in filaments and nodes of the cosmic web

Noelia R. Perez,^{1*} Luis A. Pereyra,^{2,3} Georgina Coldwell,¹ Facundo Rodriguez,^{2,3}

Ignacio G. Alfaro^{2,3} and Andrés N. Ruiz^{2,3}

¹*Facultad de Ciencias Exactas, Físicas y Naturales, Departamento de Geofísica y Astronomía, CONICET Universidad Nacional de San Juan, Av. Roza 590 (O), J5402DCS, Rivadavia, San Juan, Argentina*

²*Instituto de Astronomía Teórica y Experimental, CONICET-UNC, Laprida 854, X5000BGR Córdoba, Argentina*

³*Observatorio Astronómico de Córdoba, UNC, Laprida 854, X5000BGR Córdoba, Argentina*

Accepted XXX. Received YYY; in original form ZZZ

ABSTRACT

The standard paradigm for the formation of the Universe suggests that large structures are formed from hierarchical clustering by the continuous accretion of less massive galaxy systems through filaments. In this context, filamentary structures play an important role in the properties and evolution of galaxies by connecting high-density regions, such as nodes, and being surrounded by low-density regions, such as cosmic voids. The availability of the filament and point critic catalogues extracted by DISPERSE from the ILLUSTRIS TNG300-1 hydrodynamic simulation allows a detailed analysis of these structures. The halo occupation distribution (HOD) is a powerful tool for linking galaxies and dark matter halos, allowing constrained models of galaxy formation and evolution. In this work we combine the advantage of halo occupancy with information from the filament network to analyse the HOD in filaments and nodes. In our study, we distinguish the inner regions of cosmic filaments and nodes from their surroundings. The results show that the filamentary structures have a similar trend to the total galaxy sample indicating that, although the filaments span a wide range of densities, they may represent regions of average density. In the case of the nodes sample, an excess of faint and blue galaxies is found for the low-mass nodes suggesting that these structures are not virialised and that galaxies may be continuously falling through the filaments. Instead, the higher-mass halos could be in a more advanced stage of evolution showing features of virialised structures.

Key words: large-scale structure of Universe – methods: statistical – galaxies: halos – galaxies: statistics

1 INTRODUCTION

In the current Standard Model of Cosmology, Λ Cold Dark Matter (Λ CDM) baryons and dark matter accounts roughly 30% of the total energy-matter, which are arranged in a complex and massive network known as the “Cosmic Web” (de Lapparent et al. 1986; Bond et al. 1996). The web pattern is composed of nodes, filaments and voids, and its study allows us to understand the evolutionary process of the Universe. Filaments are traced by galaxies and transport matter from the voids to the nodes (Zel’dovich 1970; Cautun et al. 2014). Nodes are typically found in regions of high density and voids inhabit regions of significantly lower density. As for filaments, they span a wide range of densities, from superdense regions (though lower than nodes) to subdense regions (though higher than voids). The density threshold is therefore not sufficient to characterise a particular cosmic environment (Cautun et al. 2014).

In this context, Shandarin & Zeldovich (1989) suggest that dark matter halos are formed from initial density perturba-

tions in the density field of the early Universe and grow with time due to gravitational instability (Lifshitz 1946; Peebles 1980). Later, when these perturbations are dissociated from the expansion, they collapse into dark matter halos, which continue to accrete material through hierarchical clustering by continuously merging smaller structures. (White & Rees 1978; White 1994).

The galaxy formation and evolution are influenced by the environment, so it is expected that the large-scale surrounding affects their properties. Several works reveal the impact of these structures on galaxy shape and spin alignment (Faltenbacher et al. 2002; Trujillo et al. 2006; Aragón-Calvo et al. 2007; Tempel et al. 2013; Tempel & Libeskind 2013; Forero-Romero et al. 2014; Zhang et al. 2015; Ganeshiah Veena et al. 2018, 2019; Wang et al. 2020; Lee & Moon 2023), and on properties such as galaxy stellar masses, star formation rate and colour (Weinmann et al. 2006; Einasto et al. 2008; Lietzen et al. 2012; Darvish et al. 2016; Malavasi et al. 2017; Kraljic et al. 2018; Laigle et al. 2018).

The formation and evolution of galaxies in dark matter halos depend on a variety of physical processes, and also be-

* E-mail: noeliarocioperez@gmail.com (NP)

cause their properties are related to the host halo features. In this respect, it is not possible to determine exactly how galaxies populate the dark matter halos in which they reside. The Halo Occupation Distribution (HOD) model empirically links galaxies and dark matter halos, characterising the probability distribution $P(N|M)$ that a virialized halo of mass M contains N galaxies of previously determined characteristics (Peacock & Smith 2000; Berlind & Weinberg 2002; Berlind et al. 2003; Zheng et al. 2005; Guo et al. 2015; Rodriguez et al. 2015; Rodriguez & Merchán 2020). Moreover, Peacock & Smith (2000) argued that the distribution of galaxies within the halo density field depends on their position and the number of objects within the host halo. In this sense, the HOD formulation assumes that the host halo mass is the leading property that influences the galaxy properties (White & Rees 1978), although the spatial distribution of galaxies also depends on other properties (formation time, spin, concentration, neighbour mass, large-scale structure), known as the assembly bias (Gao et al. 2005; Gao & White 2007; Mao et al. 2018; Salcedo et al. 2018; Musso et al. 2018; Ramakrishnan et al. 2019; Mansfield & Kravtsov 2020).

The HOD framework has been useful in constraining models of galaxy formation and evolution (Berlind et al. 2003; Kravtsov et al. 2004; Zehavi et al. 2018), and cosmological models (van den Bosch et al. 2003; Zheng & Weinberg 2007) throughout the study of the dependence of the galaxy population properties (Berlind et al. 2003; Zheng et al. 2005; Contreras et al. 2013; Borzyszkowski et al. 2017; Zehavi et al. 2018; Yuan et al. 2022), and clustering variations with respect to large-scale environments (Artale et al. 2018; Zehavi et al. 2018; Alfaro et al. 2020; Alfaro et al. 2021; Alfaro et al. 2022). Furthermore, by characterising the evolution of the clustering (Contreras & Zehavi 2023), interpreting the clustering data (Kim et al. 2009; Ross et al. 2010; Zehavi et al. 2011) and creating mock catalogues (Grieb et al. 2016) the halo population can be better understood.

We stress that our aim in this paper is to identify any differences that may exist for HODs in different cosmic web structures, taking into account a wide range of magnitude thresholds. We are also exploring the HOD considering different galaxy properties such as colour, star formation and morphology, in order to provide a comprehensive characterisation. This paper is structured as follows: in Section 2 we summarise the data and describe the criteria for selecting samples. In Section 3 we analyse the HOD variations in nodes and filamentary structures, and their respective outskirts considering different magnitude limits. In this section, we also explore and compare the HOD for these environments with their surroundings taking into account diverse galaxy properties. Finally, in Section 4 we summarise and discuss the main results.

2 DATA

2.1 IllustrisTNG

This analysis has been based on the ILLUSTRISTNG project¹ (Marinacci et al. 2018; Naiman et al. 2018; Nelson et al.

2018; Pillepich et al. 2018a,b; Springel et al. 2018), a suite of cosmological hydrodynamic simulations developed from the original ILLUSTRIS simulations (Genel et al. 2014; Vogelsberger et al. 2014a,b) and executed with the AREPO moving mesh code (Springel 2010). The cosmological parameters are in agreement with Planck 2015 results (Planck Collaboration et al. 2016): $\Omega_{m,0} = 0.3089$, $\Omega_{\Lambda,0} = 0.6911$, $\Omega_{b,0} = 0.0486$, $h = 0.6774$, $n_s = 0.9667$ and $\sigma_8 = 0.8159$. The project has three sizes of physical simulation boxes, each with a side length of approximately 50, 100 and 300 Mpc, named TNG50, TNG100 and TNG300, respectively.

In particular, we used TNG300-1 because its higher resolution makes it the most suitable simulation for studying large-scale structures. TNG300-1 employs 2500^3 dark matter particles and 2500^3 gas particles with masses of $5.9 \times 10^7 M_\odot$ and $1.1 \times 10^7 M_\odot$, respectively, in a box of $205 h^{-1} \text{Mpc}$. There are 100 snapshots available and each one is associated with a group catalogue containing halos and subhalos. Halos (also named FoF Halo, FoF Group or Group) are found using the friend-of-friend algorithm (Huchra & Geller 1982) with linking length $b = 0.2$ and the SUBFIND algorithm (Springel et al. 2001) is used to identify subhalos (also known as Subfind Group, Subgroup or Galaxies)

2.2 DisPerSE

The Discrete Persistent Structures Extractor, DISPERSE² (Sousbie 2011; Sousbie et al. 2011; Sousbie 2013) is a multi-scale identifier of structures based on discrete Morse theory. According to this theory, the Cosmic Web can be characterised in a mathematical equivalent called the Morse complex.

Initially, the algorithm generates the density field of a discrete set of points through the Delaunay Tessellation Field Estimator (DTFE, Schaap & van de Weygaert (2000); van de Weygaert & Schaap (2009)). This allows the identification of critical points, i.e. points where the density gradient is zero (maxima, minima and saddle points). Then, Morse's theory uses mathematical properties that describe the relationship between topology and the geometry of the density field. The critical points together with their ascending and descending manifolds 0, 1, 2 and 3 can be related to clusters, filaments, walls and voids, respectively. To quantify the importance of the topological features found, the user can select the persistence level for filtering the Poisson sample noise and intrinsic uncertainty within the data set.

For this work, we use the filaments and point critics catalogues developed by Duckworth et al. (2020a,b)³ using the DISPERSE code, and available for TNG300-1. To build these catalogues, the authors selected subhalos with masses higher than $M_* > 10^{8.5} h^{-1} M_\odot$ and set the persistence parameter $\sigma = 4$ to remove spurious filaments. The catalogues are available for 8 snapshots between $z = 0$ and $z = 2$ and provide the cosmic web distances between each subhalo to the nearest minimum critical point, the nearest 1-saddle point, the nearest 2-saddle point, the nearest maximum crit-

¹ <https://www.tng-project.org/>

² <http://www2.iap.fr/users/sousbie/web/html/index888d.html?archive>

³ https://github.com/illustristng/disperse_TNG

Table 1. Percentage of halos and subhalos in each sample.

	Filaments	Nodes	Filament outskirts	Node outskirts	Unclassified
	(per cent)	(per cent)	(per cent)	(per cent)	(per cent)
Halos	29.57	3.31	20.46	3.79	42.87
Subhalos	29.23	30.71	13.32	2.81	23.93

ical point and the nearest filament segment (see for instance [Duckworth et al. \(2020a\)](#)).

2.3 Sample selection

The sample used in this paper was constructed from the TNG300-1 Groupcat at $z = 0$ by selecting subhalos with $M_* > 10^{8.5} h^{-1} M_\odot$, in agreement with the filament catalogue, contained in halos with masses $M_{200} \geq 10^{11} h^{-1} M_\odot$, where M_{200} is the mass enclosed within a region that encompasses 200 times the critical density. The purpose of this selection is to obtain well-resolved halos with about 10^3 particles. The final catalogue contained 212749 halos and 264407 subhalos.

With the aim of determining any existing differences in the halo occupation with respect to the a variety of cosmic environments we have separated the halos according to whether they belong to regions such as nodes and filaments, respectively.

In the following, we will refer to nodes as halos with a distance to maxima (peaks of the DisPerSE density field) less than R_{200} ($d_n \leq 1R_{200}$), where R_{200} is the comoving radius of a sphere centred on the halo whose mean density is 200 times the critical density of the Universe. Meanwhile, for the filaments sample, we selected halos with distance to the node $d_n > 1R_{200}$ and distance to the filament axis $d_f \leq 1h^{-1} \text{Mpc}$. This value was chosen to ensure that the objects belong to the filament core ([Galárraga-Espinosa et al. 2022, 2023](#)).

To associate each halo and subhalo with a certain environment, we determined the distances from these objects to the nearest node and filament axis. Table 1 summarises the percentage of halos and subhalos for each defined sample. The outskirts sample definitions are described in sections 3.1 and 3.2. In addition, we show the percentages of halos and subhalos not selected as part of our definitions in this work (Unclassified). We can observe that approximately half of the halos are found in filament environments (filaments and filament outskirts), less than 10% of the halos inhabit node regions (nodes and node outskirts) and the rest are found in structures not considered in this work. This result is in agreement with [Cautun et al. \(2014\)](#); [Ganeshiah Veena et al. \(2019\)](#), who found that the dark matter fraction is contained in filaments, walls, voids and nodes with 50, 25, 15 and 10 per cent, respectively. Although in the mentioned works, the fractions are calculated using the particles and not from the halos.

3 ANALYSIS

The HOD allows us to statistically determine how many galaxies inhabit halos with a mass within a given range ([Berlind & Weinberg 2002](#)). In this line, [Alfaro et al. \(2020\)](#) studied the HOD for central and satellite galaxies in very

low-density environments, given by cosmic voids. They found a significant dependence of the halo occupation behaviour with the mass and luminosity of the galaxies. In addition, [Alfaro et al. \(2021\)](#) studied the HOD in a set of future virialised superstructures (FVS, [Luparello et al. \(2011\)](#)) identified on a cosmological semi-analytic simulation to analyse the occupation of galaxies in halos within globally high-density regions. The authors found that the HOD from high-mass halos significantly increases towards the central regions of these superstructures.

In this section, we describe the procedure for the measurement of the HOD in different cosmic web structures, from the samples selected from the catalogues of the filament and point critics ([Duckworth et al. 2020a,b](#)) as described in the previous section, and explore its dependence on several galaxy properties. To estimate the HOD, we compute the mean number of galaxies per halo mass bins, $\langle N_{\text{gal}} | M_{\text{halo}} \rangle$, considering different ranges of r -band absolute magnitude for the subhalo. The error bars were determined using the jackknife technique ([Quenouille 1949](#); [Tukey 1958](#)).

Following [Alfaro et al. \(2020\)](#), we use different absolute magnitude limits to compare the behaviour of faint and bright galaxies in the HOD. We selected the r -band because it is an estimator of stellar mass and could be compare with the observational data. The magnitude values used correspond to SubhaloStellarPhotometrics catalogue ([Nelson et al. 2018](#)). In Figure 1, the HODs are shown for the total, nodes and filaments samples considering the following r -magnitude thresholds: $M_r - 5\log_{10}(h) \leq -17, -18, -19$ and -20 . The lower sub-panels show the quotient between the nodes and filaments samples with respect to total HOD. As expected, the halo occupancy decreases when we consider increasingly brighter subhalos. The HOD for halos belonging to filaments is quite similar to that shown for the total sample, independent of galaxy luminosity. An increase in error can be observed for halos with masses higher than $10^{14.5} h^{-1} M_\odot$.

On the other hand, for the nodes sample, there is a significant excess of faint galaxies compared to the filaments and total samples. The main difference in the HOD between the samples occurs for halos with masses lower than $10^{13} h^{-1} M_\odot$, where we see that the HOD measured for the nodes is approximately two times higher than that measured for the filaments for the magnitude limit: $M_r - 5\log_{10}(h) \leq -17$. This discrepancy decreases and becomes imperceptible as we look at brighter galaxies, so this dependence on the magnitude thresholds could be related to the presence of satellite galaxies in the lower-mass halos. The distributions for halos with masses $M_{\text{halo}} > 10^{13} h^{-1} M_\odot$ are comparable. The error bars in the extreme regions, especially for the filaments sample, is related to the fact that there are few massive halos in these structures, so the last bins are almost free of objects.

It is important to highlight that the differences in the node HOD measurements are more noticeable for the magnitude threshold $M_r - 5\log_{10}(h) \leq -17$. It is worth noting that we find in our nodes a different effect than [Alfaro et al. \(2021\)](#) in high-density regions (FVSs). They found a luminosity-independent increase in the mean number of satellites from halos with masses above $\sim 10^{13} h^{-1} M_\odot$. Meanwhile, nodes HODs show differences in low-mass halos and exhibit a luminosity dependence. Then, in order to be able to carry out a more detailed analysis within this luminosity range, we have set this limit at the following analysis. Since the dif-

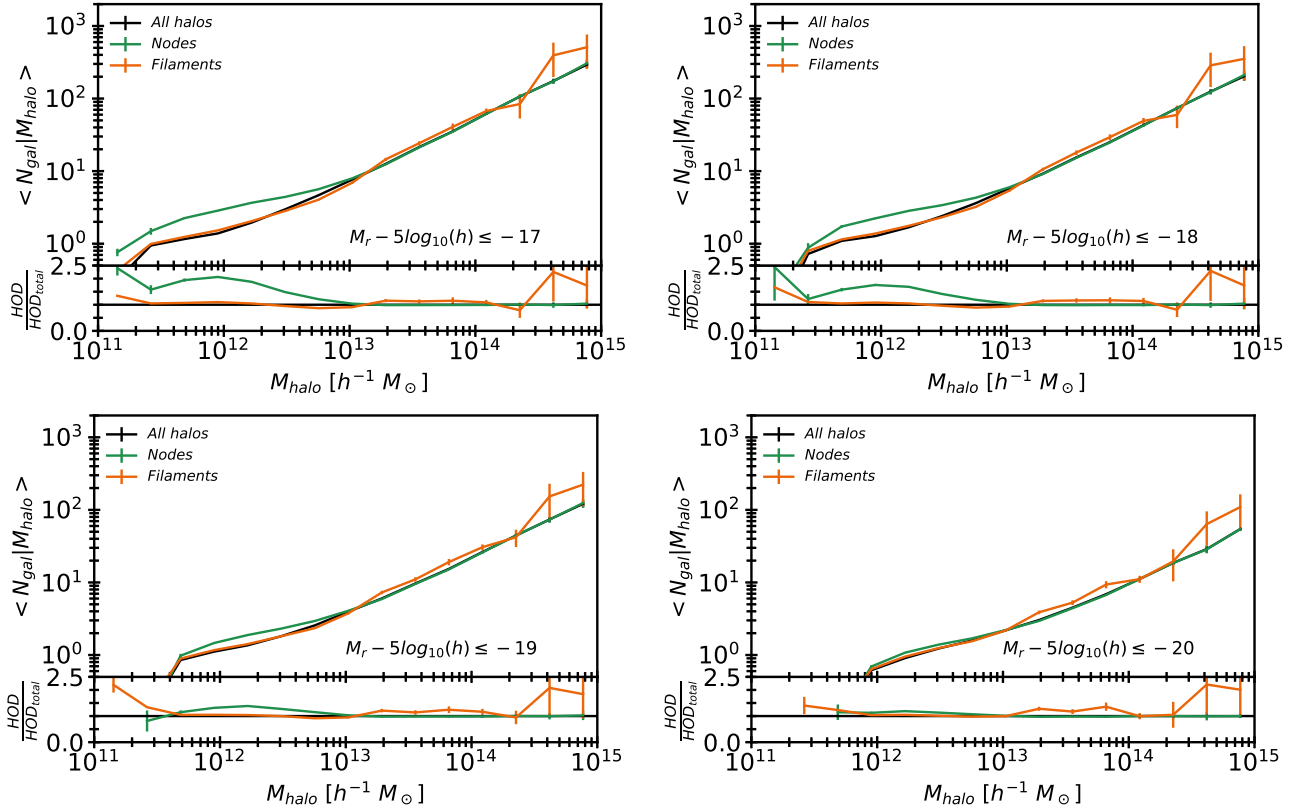


Figure 1. The panels show the HODs measured for galaxies with different magnitude thresholds for the whole sample (black lines) and for galaxies belonging to filaments (orange lines) and nodes (green lines), respectively. Lower sub-panels show the ratio between the HOD inside filaments and nodes and the HOD in the whole sample.

ferences detected in the HODs could be related to the properties of the galaxies, we performed an exhaustive analysis using galaxy colours since this property provides us with information on morphology, age and evolution (Blanton et al. 2005; Vulcani et al. 2015).

In Fig. 2 we plotted the galaxy colour distributions for filaments, nodes and total samples considering the halo mass bins. In accordance with Nelson et al. (2018), the general tendency suggests that low-mass halos are mainly populated by blue galaxies, with a small contribution from the red ones. Furthermore, as the halos become more massive, the number of red galaxies increases while the number of blue galaxies gradually decreases. Finally, massive halos are populated by red galaxies, suggesting the presence of a more evolved population. Regarding the nodes and filaments samples, for massive halos, the galaxy colours in both samples are comparable to the total sample. As for the low-mass halos, we found that the filaments sample follows the overall trend, whereas the nodes sample shows a remarkable bimodal colour distribution. This behaviour could be explained by the fact that the low-mass nodes represent local density maxima in the cosmic web inhabited by galaxies groups, which show evidence of physical processes that redden them even before they reach the virial radius (Blanton et al. 2003; Kraljic et al. 2018).

The evolutionary history of galaxies can be inferred from the SFR parameter, which is related to the amount of gas and the efficiency of star formation (Kennicutt 1998). Several processes at scales between parsecs and Megaparsecs affect

star formation (Kennicutt & Evans 2012), such as environment and galaxy mass (Kauffmann et al. 2004; Peng et al. 2010; Moutard et al. 2018). To complement the analysis, we determine the morphology using the supplementary catalogue of stellar circularities, angular momentum, and axis ratios (Genel et al. 2015). The morphology, together with colour and SFR, allows us to characterise the galaxy properties within specific halos. The correlation between these parameters indicates that late blue galaxies have a higher SFR than early red galaxies (e.g. Schawinski et al. (2014)).

In order to calculate the HODs, we separate the subhalos with respect to the parameters mentioned above. Following Pillepich et al. (2019), we calculate recursively star forming main sequence (SFMS) ridge line in the SFR vs. stellar mass plane. Then, we define star-forming and quiescent galaxies as those above and below the SFMS line, respectively. To exploit the bimodality of galaxy colours, we choose a value of $M_g - M_r = 0.6$ as the cut-off to distinguishing red ($M_g - M_r > 0.6$) from blue ($M_g - M_r \leq 0.6$) galaxies (Nelson et al. 2018). Finally, to define disk (spheroidal) galaxies, we use the circularity parameter as a criterion, defining the bulge mass fraction as twice the stellar mass fraction with a negative circularity parameter lower (higher) than 0.5 (see e.g. Osato & Okumura (2023)).

In the next subsections, we analyse the HODs for filaments, nodes and their surrounding regions separately, in order to study both environments in more detail.

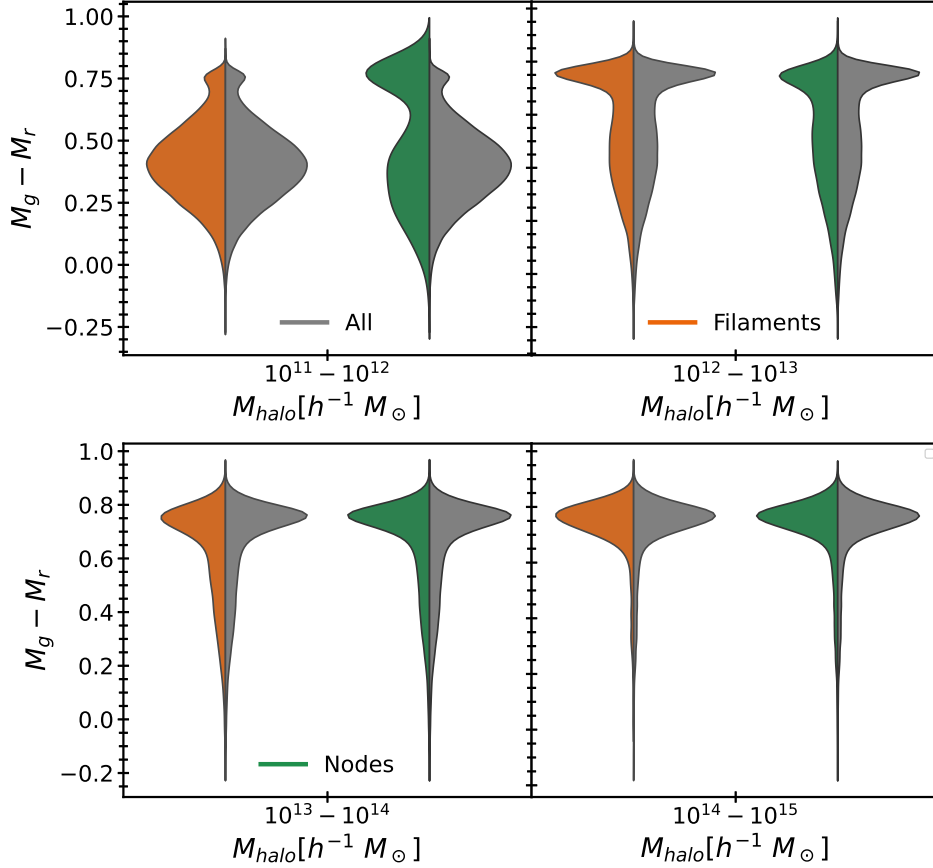


Figure 2. Galaxy colour distributions, in the halo mass bins, for the total sample (grey), the filaments sample (orange) and the nodes sample (green).

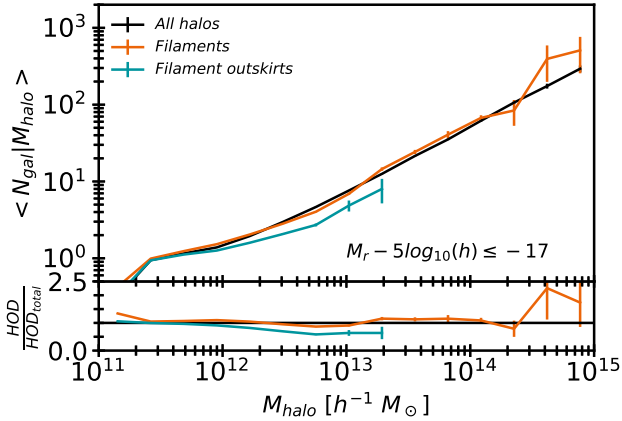


Figure 3. HODs measured for the total (black), filaments (orange) and filament outskirts (light-blue) samples for subhalos with $M_r - 5 \log_{10}(h) \leq -17$. Sub-panel: the ratio between the filaments and filament outskirts samples respect to the overall HOD.

3.1 Filaments

Taking into account the previous results, in this subsection we have focused on the analysis of the HOD in filamentary structures, considering both filaments and filament outskirts in order to account for their variations with respect to the filament distances. Then, we consider the filaments sample,

which remains unchanged, and the filament outskirts sample defined by selecting halos with $d_n > 1 R_{200}$ to exclude the nodes and $1 < d_f [h^{-1} \text{Mpc}] \leq 2$, considering an intermediate region between filaments and voids. The number of halos and subhalos in each sample is given in Table 1.

The HODs for filaments and filament outskirts are shown in Figure 3. It can be observed that for halo masses smaller than $10^{12} h^{-1} M_{\odot}$ the tendency of both samples is similar following the overall trend. This fact suggests that the process by which galaxies populate these halos may be similar, regardless of the environment. For $M_{\text{halo}} > 10^{12} h^{-1} M_{\odot}$, the HODs for the filaments and the total samples are indistinguishable, within the errorbars, while for the filament outskirts sample the curve is lower and corresponds to an environment without the presence of massive halos. This result is in agreement with the trend found by Alfaro et al. (2020), who studied the HOD in environments with 10 per cent of the mean density of large scale tracers, reaching a halo mass of $\approx 10^{13} h^{-1} M_{\odot}$, a similar mass range to the filament outskirts. Furthermore, they found that for halos more massive than $10^{12} h^{-1} M_{\odot}$, the HOD in voids it is up to 50% lower than the overall trend.

On the other hand, we explore the galaxy colour distributions, with respect to halo mass bins, for filaments and their outskirts samples. In Figure 4 it can be seen that both environments have comparable distributions for $M_{\text{halo}} < 10^{13} h^{-1} M_{\odot}$. Also, for masses in the range $10^{13} < M_{\text{halo}} [h^{-1} M_{\odot}] < 10^{14}$, the samples suggest that the galaxies

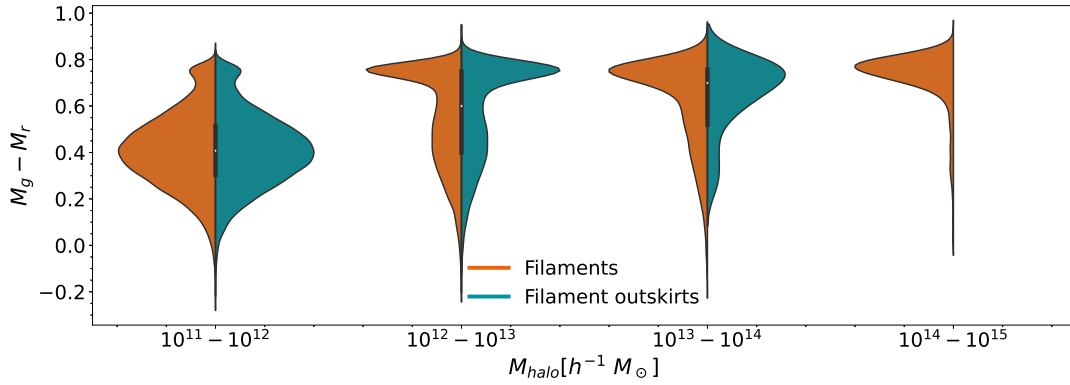


Figure 4. Colour distributions of galaxies in halo mass bins for filaments (orange) and filament outskirts (light-blue) samples.

are predominantly red, although the distribution of the filament outskirts shows a higher dispersion with respect to the filament distribution. Furthermore, these surrounding regions do not have halos with masses higher than $10^{14} h^{-1} M_{\odot}$, as mentioned earlier.

Progressing with the analysis of HODs in terms of galaxy properties we study, in Figure 5, the HODs for blue ($M_g - M_r \leq 0.6$) and red ($M_g - M_r > 0.6$) galaxies for each sample. As expected, the low-mass halos are preferentially populated by blue galaxies, in contrast to the high-mass halos dominated by red galaxies. The tendencies of the red galaxies for the two samples are close to each other and lie on the distribution of the total red galaxies. This suggests that the halo occupation by red galaxies is similar in both environments. On the other hand, an apparent disparity is observed when blue galaxies are considered. While the filaments sample tends to approximate the total blue sample within the error bars, the surrounding regions, corresponding to the filaments outskirts, show a slight decrease in blue galaxies as we consider more massive halos. This result may be biased due to the combination of the effect of the colour-density segregation (Kraljic et al. 2018) and our filament environments definition.

Taking into account the SFR parameter described in the previous section, the HODs of quiescent and star-forming galaxies, obtained by considering the mean value of the SFR parameter, are shown in Figure 6. Looking at the quiescent galaxies, we observe that the filaments sample lies on the total distribution of inactive galaxies. For high-mass halos, the behaviour shows scattering caused by the low number of objects in these mass bins. The filament outskirts show a similar trend to the filaments sample but with a lower distribution, indicating the presence of fewer inactive galaxies. On the other hand, for low-mass halos, we observe that the star-forming galaxies in the filaments sample have a HOD similar to the total of the star-forming galaxies, while for high-mass halos the behaviours show a sinusoidal shape with respect to this distribution. Besides, halos in the filament outskirts are practically devoid of star-forming galaxies. In contrast, several works based on different galaxy surveys have found that massive and/or quiescent galaxies are found closer to the filament axis than low-mass and/or star-forming galaxies, which prefer to inhabit the filaments outskirts (Malavasi et al. 2017; Kraljic et al. 2018; Laigle et al. 2018; Bonjean et al. 2020).

To conclude the analysis of the HOD taking into account

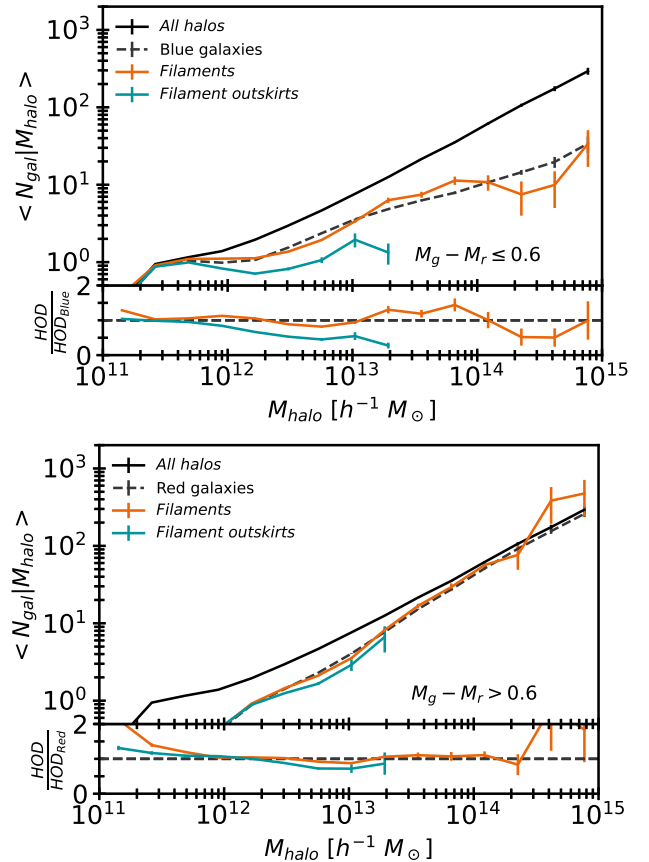


Figure 5. Panel shows the measured HOD with respect to the galaxy colours for the total (black), filaments (orange) and filament outskirts (light-blue) samples for galaxies with $M_r - 5 \log_{10}(h) \leq -17$. The dashed lines represent the HODs for the total of blue (upper) and red (lower) galaxies. The lower sub-panels show the ratio of the filaments and filament outskirts samples to the total number of blue and red galaxies, respectively.

the galaxy properties, we show the distributions with respect to morphology, as described in previous section, in Figure 7. The HODs for both filaments samples are comparable to the global trends, and although the HODs for filament outskirts are lower for both morphologies, the halo occupation is significantly lower for disk galaxies.

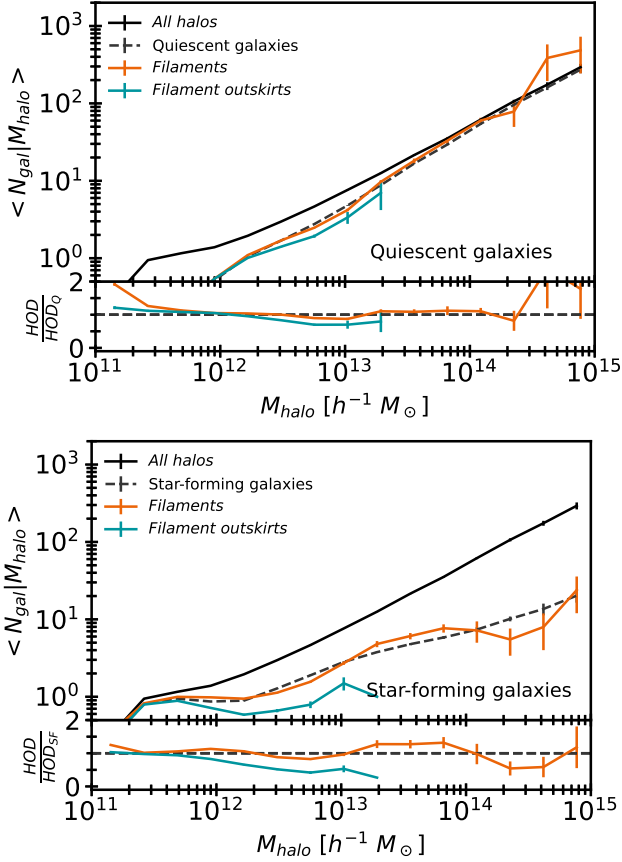


Figure 6. Panels shows the HODs measured with respect to the subhalo star formation rate parameter (SFR) for the total (grey), filaments (orange) and filament outskirts (light-blue) samples for subhalos with $M_r - 5\log_{10}(h) \leq -17$. The dashed lines represent the HODs for the total of quiescent (upper) and star-forming (lower) subhalos. Lower sub-panels show the ratio between the filaments and filament outskirts samples with the total of quiescent and star-forming subhalos, respectively.

The HODs measurements for the filaments sample, taking into account the studied galaxy properties, show that the halo occupancy in these environments is quite similar to the general trend, while halos belonging to the filament outskirts show HODs up to 0.5 times lower than the general trend, despite the considered property. It is important to note that our definition of filament environment does not take into account the filament radius according to its density profile. These definitions could lead to different biases in the HOD. For example, red galaxies distribution are preferably locate nearest to filament spine while the blue galaxies inhabit the voids surrounding. This effect explains the discrepancy in the outskirts filament environment concerning other works.

3.2 Nodes

For the sake of consistency, we apply the analysis of the previous subsection to the environments corresponding to the nodes sample. To account for HOD variations in the environment associated with such cosmic web structures, we have also constructed a sample of the node periphery, called node outskirts, by selecting halos with $1 < d_n [R_{200}] \leq 3$ to obtain

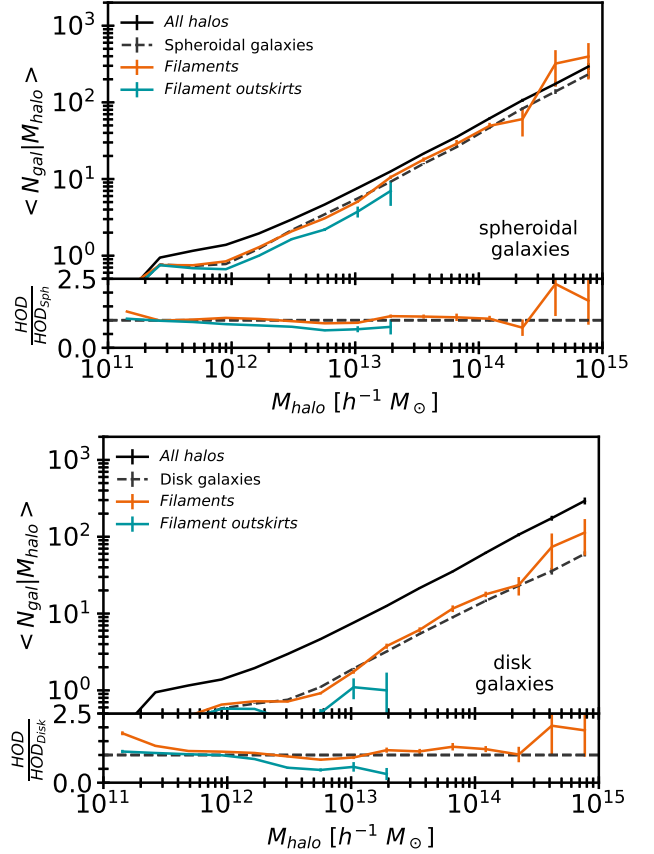


Figure 7. Panel shows the measured HOD with respect to the subhalo morphology for the total (black), filaments (orange) and filament outskirts (light-blue) samples for subhalos with $M_r - 5\log_{10}(h) \leq -17$. The dashed lines represent the HODs for the total of spheroidal (upper) and disk (lower) subhalos. Lower sub-panels show the ratio between the filaments and filament outskirts samples with the total of spheroidal and disk subhalos, respectively.

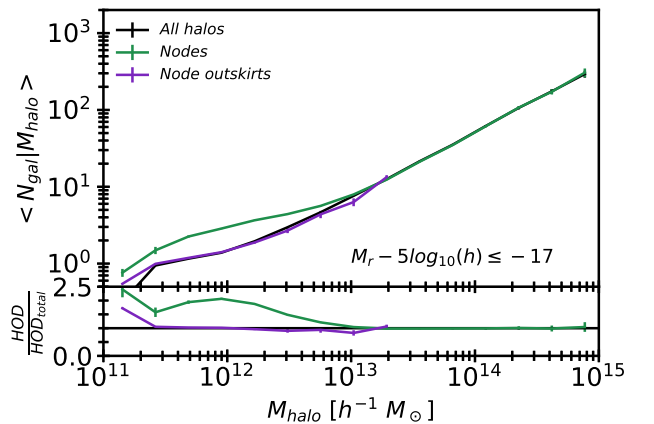


Figure 8. HODs measured for the total (black), nodes (green) and node outskirts (purple) samples for subhalos with $M_r - 5\log_{10}(h) \leq -17$. Lower sub-panel shows the ratio between the nodes and node outskirts samples with the overall HOD.

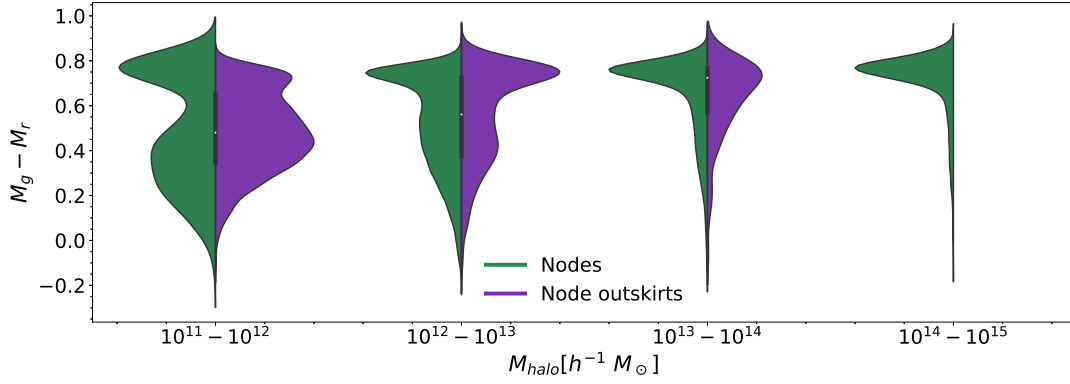


Figure 9. Galaxy colour distributions in halo mass bins for nodes (green) and node outskirts (purple) samples.

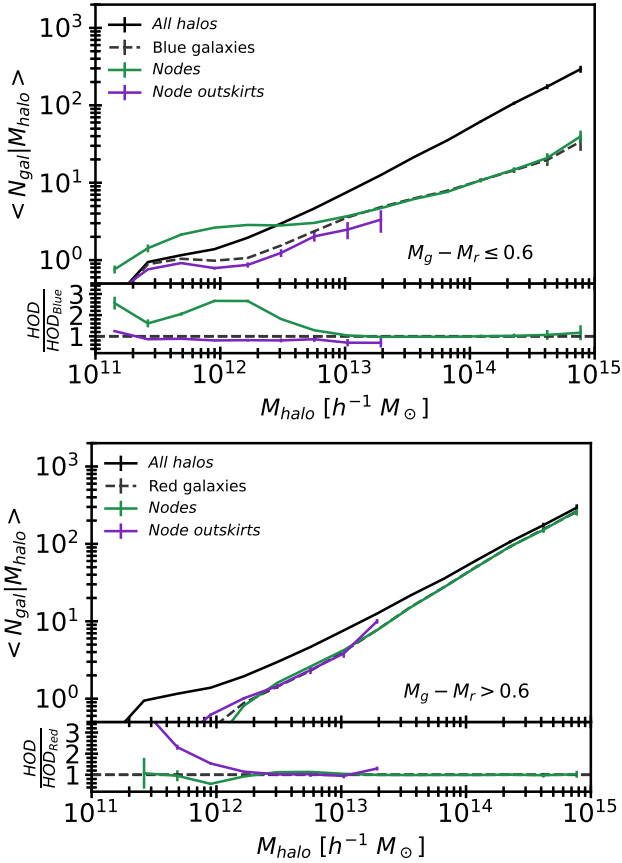


Figure 10. The main panel shows the measured HODs with respect to the galaxy colours for three samples: total (black), nodes (green), and node outskirts (purple), considering the subhalos with a magnitude of $M_r - 5\log_{10}(h) \leq -17$. The dashed lines in the upper and bottom panels represent the HODs for the total blue and red galaxies, respectively. Below each panel, we plot the ratio of the nodes and node outskirts samples with respect to the total number of blue and red galaxies

halos in the node vicinity. The number of halos and subhalos can be found in Table 1.

In Figure 8 we show the HODs for subhalos, with magnitude threshold $M_r - 5\log_{10}(h) \leq -17$, for the total, nodes and node outskirts samples. Both samples have a notable dif-

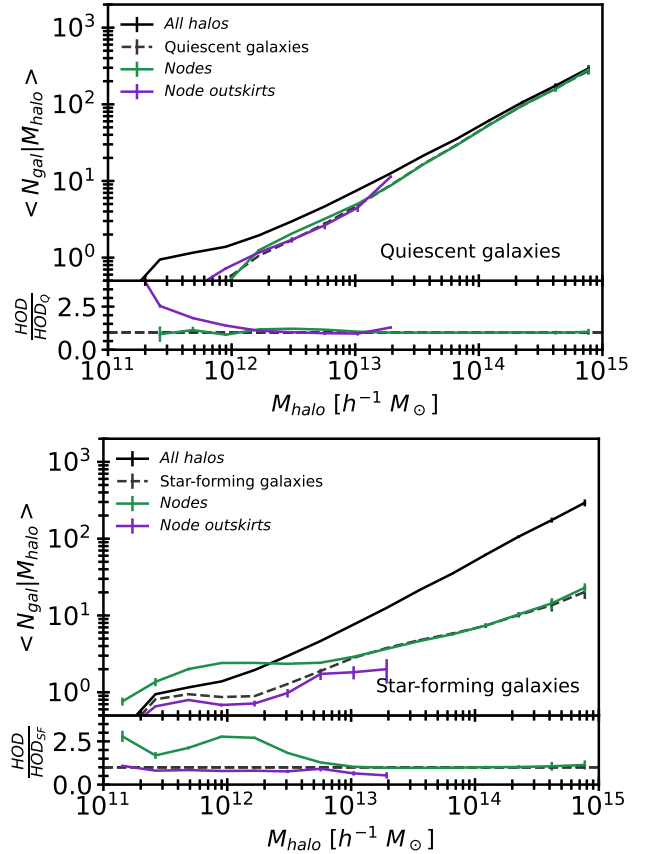


Figure 11. Panel shows the measured HOD with respect to the SFR parameter for the total (grey), nodes (green) and node outskirts (purple) samples for subhalos with $M_r - 5\log_{10}(h) \leq -17$. The dashed lines represent the HODs for the total of quiescent (upper) and star-forming (lower) subhalos. Lower sub-panels show the ratio between the nodes and node outskirts samples with the total of quiescent and star-forming subhalos, respectively.

ference for halo masses $M_{200} < 10^{13} h^{-1} M_{\odot}$, where the HOD measured for the nodes is 2.5 times higher than the trend for the node outskirts, which overlaps with the overall trend. This result suggests an excess of faint galaxies in the low-mass halo population, indicating that the low-mass halos are still in formation.

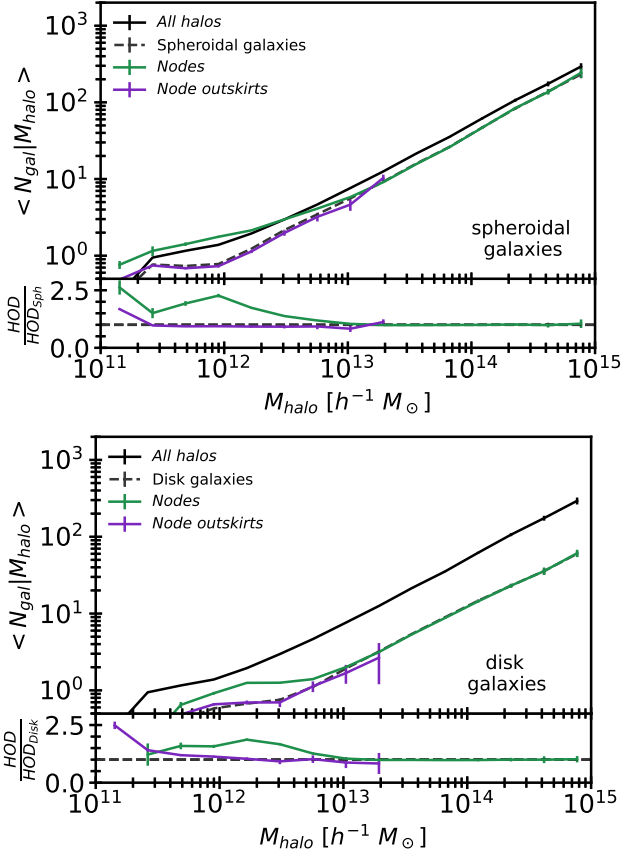


Figure 12. Panel shows the measured HODs with respect to the subhalo morphology for the total (black), nodes (green) and node outskirts (purple) samples for subhalos with $M_{\text{r}} - 5\log_{10}(h) \leq -17$. The dashed lines represent the HODs for the total of spheroidal (upper) and disk (lower) subhalos. Lower sub-panels show the ratio between the nodes and node outskirts samples with the total of spheroidal and disk subhalos, respectively.

In line with the previous subsection, we examine the galaxy colour distributions for both environments in halo mass bins. Figure 9 shows that low-mass halos in nodes exhibit a distinct bimodal colour distribution, with the red component becoming more significant as mass increases, until the blue component disappears completely for massive halos. Nevertheless, the low-mass halos within the node outskirts show a distinct colour bimodality with an overpopulation of objects in the green valley. Also, the red component becomes more significant with increasing mass. The last mass bin is empty, reflecting the reason for the mass limit in the HODs for these environments. These results are a consequence of the density environments affecting the galaxy properties. In the high mass halos in nodes the galaxies are more evolved because they have had more time to deplete the gas store and, so stop star formation becoming redder. However, for the lower halo mass in nodes, many galaxies are still being accreted then a population of young objects is observed in the bimodal distribution. In agreement with Domínguez et al. (2001) we also observe that different mechanisms control the morphological segregation depending on the galaxy environment, then in the node outskirts the lower local density allows to find a transition population, probably between field and nodes (see Fig.

2). In addition, Martínez et al. (2008) found that colour is the property that depends most on the distance from the centre of the cluster. In this sense, the overpopulation of galaxies in the green valley in halos belonging to node outskirts sample could be related to the fact that the colour of these objects is being modified in this environment.

Following the same line as the one in the previous subsection in Figure. 10 we show the HODs considering the galaxy colours. In the case of blue galaxies (upper panel), the nodes sample shows an excess of blue galaxies for halos with masses lower than $10^{13} h^{-1} M_{\odot}$ while the halos inhabiting in the node outskirts exhibit a HOD slightly lower than the average HOD, within the error bars. For the red galaxies (lower panel), the trends for the HODs for both samples (nodes and their outskirts) are similar and lie close to the distribution of the total red galaxies.

In addition, in Figure 11 we show the HODs taking into account the SFR parameter. In the upper panel we observe the HODs for quiescent galaxies. The distributions of both samples lie on the HOD for total inactive subhalos. Finally, the lower panel shows the distributions for star-forming galaxies. Low-mass halos in nodes have an excess of star-forming galaxies over the total active galaxies, which is even higher than the total feature, then for massive halos the HOD decreases and is placed on the trend of the total star-forming galaxies. On the contrary, halos in the regions surrounding the nodes have a lower distribution than the total active galaxy distribution for the whole range of masses.

Finally, in Figure 12 we show the HODs as a function of the galaxy morphology. The HODs calculated with spheroidal galaxies indicate that low-mass halos in nodes have an excess of early-type galaxies with respect to the total sample. In the intermediate mass range, the distribution decreases until it overlaps with the HOD for a total of spheroidal galaxies. On the other hand, the node outskirts sample coincides with the total early-type galaxies distribution, regardless of halo mass. For disk galaxies, the HOD for node halos is higher than the total distribution of disk galaxies in the low-mass region, but both samples overlap in the high-mass halo region. The HOD for halos in the vicinity of nodes is close to the total distribution of disk galaxies, with a slight difference in the low-mass halo range.

The HODs measured for the nodes sample show an excess of faint, blue and star-forming galaxies for low-mass halos. Regarding to the morphology, the HODs show an excess of spheroidal and disk galaxies in the lower mass range. These trends could be related to the measurement of the circularity parameter for low-mass galaxies, which have few stars to obtain an accurate result (Abadi et al. 2003). On the other hand, the halo occupancy in the node outskirts is quite similar to the overall trend, regardless of the property considered.

4 SUMMARY AND CONCLUSIONS

We have performed the Halo Occupation Distribution (HOD) measurements for halos derived from Groupcat at $z = 0.00$ from ILLUSTRIS TNG300-1 simulations. Firstly, we separated halos belonging to filaments and nodes, taking into account the distance to the node and to the filament axis. The nodes sample was constructed by considering halos with distance to the node $d_n \leq 1 R_{200}$ and for the filaments sam-

ple we selected halos with distance to the node $d_n > 1 R_{200}$ and distance to the filament axis $d_f \leq 1 h^{-1}\text{Mpc}$.

We compute the mean number of galaxies per halo mass bin for the total, nodes and filaments samples considering four magnitude thresholds: $M_r - 5\log_{10}(h) \leq -17, -18, -19$ and -20 and find that the HOD decreases when we consider increasingly brighter galaxies. Furthermore, the HOD for halos in filaments is similar to that shown for the total sample, regardless of galaxy luminosity, while the nodes sample shows a significant excess of faint galaxies at lower halo masses, which decreases for bright galaxies. Since the differences in the HOD measurements are more pronounced for the $M_r - 5\log_{10}(h) \leq -17$ magnitude limit, we have chosen this cut-off magnitude for a more detailed analysis in the following.

The colour distribution of the total sample suggests that the galaxies in low-mass halos are bluer and, as mass increases the galaxies become redder. The filaments and nodes samples follow the general trend, except for low-mass halos associated with nodes, which have a bimodal colour distribution. Later, we measure the HODs taking into account several galaxy properties such as colour, star formation rate (SFR) and morphology in filaments, nodes and their surrounding regions.

Then, in order to study the variations associated with the distance to filamentary structures we define a filament outskirts sample by selecting halos with $d_n > 1R_{200}$ and $1 < d_f [h^{-1}\text{Mpc}] \leq 2$. The HODs for subhalos with $M_r - 5\log_{10}(h) \leq -17$ show that the filaments follow the overall trend, while the filament outskirts sample with $M_{\text{halo}} > 10^{12} h^{-1}M_{\odot}$ is 0.5 times lower than the total, suggesting that these less dense environments are less likely to be inhabited by galaxies. This result is in agreement with [Alfaro et al. \(2020\)](#), who found similar trends for even less dense regions. Looking at galaxy colours, despite the absence of massive halos in the outskirts, the galaxy colour distributions are quite similar in both samples. The calculated HODs, discriminating the galaxy colours, show that the halo occupation of red galaxies is quite similar in both environments, while blue galaxies are less likely to be found in the outskirts than in the filaments for halo masses $M_{\text{halo}} > 10^{12} h^{-1}M_{\odot}$. Moreover, using the SFR parameter to measure HODs, we found that the tendency of quiescent and star-forming galaxies to inhabit halos associated with filaments is similar to the global trends. The filament outskirts show fewer inactive galaxies than the filaments and are devoid of star-forming galaxies. In terms of morphology, the HODs show that the halos in the filaments are populated by disk and spheroidal galaxies, similar to the overall trend, while the outskirts are generally devoid of galaxies, although they have significantly fewer disk galaxies.

Following the study in the filamentary regions, we examined the nodes and their surrounding regions. The node outskirts sample was built considering halos with $1 < d_n [R_{200}] \leq 3$. Taking into account the magnitude limit $M_r - 5\log_{10}(h) \leq -17$, we observe a remarkable excess of faint galaxies in the halo occupation for halos with masses lower than $10^{13} h^{-1}M_{\odot}$, while the outskirts follow the global trend. The galaxy colour distributions for low-mass halos are bimodal, and with increasing mass the red component becomes more significant in both samples, although there are no massive halos in the outskirts. The HODs with respect

to galaxy colours show an excess of blue galaxies for halos with masses lower than $10^{13} h^{-1}M_{\odot}$ in the nodes, while the node outskirts show a halo occupation slightly lower than the total sample. The HODs measurement, taking into account the SFR parameter, suggests an excess of star-forming galaxies for halos with $M_{\text{halo}} < 10^{13} h^{-1}M_{\odot}$ belonging to nodes, and for massive halos the occupancy is quite similar to the overall trend. The HOD for quiescent galaxies lies on the total distribution of inactive galaxies. In the node outskirts, the quiescent galaxies show an halo occupancy comparable to the overall trend, and the star-forming galaxies have a lower occupancy than the total tendency. Regarding morphology, the HODs for nodes show an excess of both, disk and bulge galaxies, for nodes with masses lower than $10^{13} h^{-1}M_{\odot}$, while the halos within the node outskirts have an occupancy comparable to the global trend.

The halo occupation in filaments appears to be independent of the properties of the galaxies inhabiting these environments and similar to the global tendency. Instead of that the outskirts of the filaments show a lower halo occupancy. Regarding the nodes, the HODs for low-mass halos show a significant difference with respect to the other samples. In this sense, the nodes could represent structures where the galaxies fall through the filaments, and they could be at different stages of evolution depending on their mass. These results could be related to the halo assembly bias, as proposed by [Ramakrishnan et al. \(2019\)](#) and [Mansfield & Kravtsov \(2020\)](#), who consider this important issue for the formation and evolution of the large structures of the Universe. Also, works such as [Borzyszkowski et al. \(2017\)](#) point out that such a bias is a product of the action of large structures in the Universe that cause the extinction of halo growth through tidal forces. In particular, they claim that ‘‘stalled’’ halos would be found at the nodes. The changes we observe in the HOD could result from just such a difference in the formation history of halos.

The analysis performed in this work allows us to obtain information about the processes by which galaxies populate the halos in the large structures of the Universe, and how these processes affect the properties of the galaxies. The study of the evolution of HODs leads to a very interesting topic of analysis, as suggested by [Contreras & Zehavi \(2023\)](#). In a forthcoming work, we will then assess the evolution of HODs in the large-scale environments given by filamentary structures.

ACKNOWLEDGEMENTS

This work was supported in part by the Consejo Nacional de Investigaciones Científicas y Técnicas de la República Argentina (CONICET) and the Consejo Nacional de Investigaciones Científicas, Técnicas y de Creación Artística de la Universidad Nacional de San Juan (CICITCA). The authors would like to thank the ILLUSTRISTNG team for making their data available to the public. FR would like to acknowledge support from the ICTP through the Junior Associates Programme 2023-2028.

DATA AVAILABILITY

The simulation data underlying this article are publicly available at the TNG website. The data results arising from this work will be shared on reasonable request to the corresponding authors.

REFERENCES

- Abadi M. G., Navarro J. F., Steinmetz M., Eke V. R., 2003, *ApJ*, **597**, 21
- Alfaro I. G., Rodriguez F., Ruiz A. N., Lambas D. G., 2020, *A&A*, **638**, A60
- Alfaro I. G., Ruiz A. N., Luparello H. E., Rodriguez F., Lambas D. G., 2021, *Astronomy & Astrophysics*, **654**, A62
- Alfaro I. G., Rodriguez F., Ruiz A. N., Luparello H. E., Lambas D. G., 2022, *A&A*, **665**, A44
- Aragón-Calvo M. A., van de Weygaert R., Jones B. J. T., van der Hulst J. M., 2007, *ApJ*, **655**, L5
- Artale M. C., Zehavi I., Contreras S., Norberg P., 2018, *MNRAS*, **480**, 3978
- Berlind A. A., Weinberg D. H., 2002, *ApJ*, **575**, 587
- Berlind A. A., et al., 2003, *ApJ*, **593**, 1
- Blanton M. R., et al., 2003, *ApJ*, **594**, 186
- Blanton M. R., Eisenstein D., Hogg D. W., Schlegel D. J., Brinkmann J., 2005, *ApJ*, **629**, 143
- Bond J. R., Kofman L., Pogosyan D., 1996, *Nature*, **380**, 603
- Bonjean V., Aghanim N., Douspis M., Malavasi N., Tanimura H., 2020, *A&A*, **638**, A75
- Borzyszkowski M., Porciani C., Romano-Díaz E., Garaldi E., 2017, *Monthly Notices of the Royal Astronomical Society*, **469**, 594
- Cautun M., van de Weygaert R., Jones B. J. T., Frenk C. S., 2014, *MNRAS*, **441**, 2923
- Contreras S., Zehavi I., 2023, *arXiv e-prints*, p. [arXiv:2305.19628](https://arxiv.org/abs/2305.19628)
- Contreras S., Baugh C. M., Norberg P., Padilla N., 2013, *MNRAS*, **432**, 2717
- Darvish B., Mobasher B., Sobral D., Rettura A., Scoville N., Faisst A., Capak P., 2016, *ApJ*, **825**, 113
- Domínguez M., Muriel H., Lambas D. G., 2001, *AJ*, **121**, 1266
- Duckworth C., Tojeiro R., Kraljic K., 2020a, *MNRAS*, **492**, 1869
- Duckworth C., Starkenburg T. K., Genel S., Davis T. A., Habouzit M., Kraljic K., Tojeiro R., 2020b, *MNRAS*, **495**, 4542
- Einasto M., et al., 2008, *ApJ*, **685**, 83
- Faltenbacher A., Gottlöber S., Kerscher M., Müller V., 2002, *A&A*, **395**, 1
- Forero-Romero J. E., Contreras S., Padilla N., 2014, *MNRAS*, **443**, 1090
- Galárraga-Espinosa D., Langer M., Aghanim N., 2022, *A&A*, **661**, A115
- Galárraga-Espinosa D., Garaldi E., Kauffmann G., 2023, *A&A*, **671**, A160
- Ganeshaiiah Veena P., Cautun M., van de Weygaert R., Tempel E., Jones B. J. T., Rieder S., Frenk C. S., 2018, *MNRAS*, **481**, 414
- Ganeshaiiah Veena P., Cautun M., Tempel E., van de Weygaert R., Frenk C. S., 2019, *MNRAS*, **487**, 1607
- Gao L., White S. D. M., 2007, *MNRAS*, **377**, L5
- Gao L., Springel V., White S. D. M., 2005, *MNRAS*, **363**, L66
- Genel S., et al., 2014, *MNRAS*, **445**, 175
- Genel S., Fall S. M., Hernquist L., Vogelsberger M., Snyder G. F., Rodriguez-Gomez V., Sijacki D., Springel V., 2015, *ApJ*, **804**, L40
- Grieb J. N., Sánchez A. G., Salazar-Albornoz S., Dalla Vecchia C., 2016, *MNRAS*, **457**, 1577
- Guo H., et al., 2015, *MNRAS*, **453**, 4368
- Huchra J. P., Geller M. J., 1982, *ApJ*, **257**, 423
- Kauffmann G., White S. D. M., Heckman T. M., Ménard B., Brinchmann J., Charlot S., Tremonti C., Brinkmann J., 2004, *MNRAS*, **353**, 713
- Kennicutt Robert C. J., 1998, *ARA&A*, **36**, 189
- Kennicutt R. C., Evans N. J., 2012, *ARA&A*, **50**, 531
- Kim H.-S., Baugh C. M., Cole S., Frenk C. S., Benson A. J., 2009, *MNRAS*, **400**, 1527
- Kraljic K., et al., 2018, *MNRAS*, **474**, 547
- Kravtsov A. V., Berlind A. A., Wechsler R. H., Klypin A. A., Gottlöber S., Allgood B., Primack J. R., 2004, *ApJ*, **609**, 35
- Laigle C., et al., 2018, *MNRAS*, **474**, 5437
- Lee J., Moon J.-S., 2023, *arXiv e-prints*, p. [arXiv:2305.04409](https://arxiv.org/abs/2305.04409)
- Lietzen H., Tempel E., Heinämäki P., Nurmi P., Einasto M., Saar E., 2012, *A&A*, **545**, A104
- Lifshitz E. M., 1946, *Zhurnal Eksperimentalnoi i Teoreticheskoi Fiziki*, **16**, 587
- Luparello H., Lares M., Lambas D. G., Padilla N., 2011, *MNRAS*, **415**, 964
- Malavasi N., et al., 2017, *MNRAS*, **465**, 3817
- Mansfield P., Kravtsov A. V., 2020, *Monthly Notices of the Royal Astronomical Society*, **493**, 4763
- Mao Y.-Y., Zentner A. R., Wechsler R. H., 2018, *MNRAS*, **474**, 5143
- Marinacci F., et al., 2018, *MNRAS*, **480**, 5113
- Martínez H. J., Coenda V., Muriel H., 2008, *MNRAS*, **391**, 585
- Moutard T., Sawicki M., Arnouts S., Golob A., Malavasi N., Adami C., Coupon J., Ilbert O., 2018, *MNRAS*, **479**, 2147
- Musso M., Cadiou C., Pichon C., Codis S., Kraljic K., Dubois Y., 2018, *Monthly Notices of the Royal Astronomical Society*, **476**, 4877
- Naiman J. P., et al., 2018, *MNRAS*, **477**, 1206
- Nelson D., et al., 2018, *MNRAS*, **475**, 624
- Osato K., Okumura T., 2023, *MNRAS*, **519**, 1771
- Peacock J. A., Smith R. E., 2000, *MNRAS*, **318**, 1144
- Peebles P. J. E., 1980, *The large-scale structure of the universe*
- Peng Y.-j., et al., 2010, *ApJ*, **721**, 193
- Pillepich A., et al., 2018a, *MNRAS*, **473**, 4077
- Pillepich A., et al., 2018b, *MNRAS*, **475**, 648
- Pillepich A., et al., 2019, *MNRAS*, **490**, 3196
- Planck Collaboration et al., 2016, *A&A*, **594**, A13
- Quenouille M. H., 1949, *The Annals of Mathematical Statistics*, **20**, 355
- Ramakrishnan S., Paranjape A., Hahn O., Sheth R. K., 2019, *Monthly Notices of the Royal Astronomical Society*, **489**, 2977
- Rodriguez F., Merchán M., 2020, *Astronomy & Astrophysics*, **636**, A61
- Rodriguez F., Merchán M., Sgró M. A., 2015, *A&A*, **580**, A86
- Ross A. J., Percival W. J., Brunner R. J., 2010, *MNRAS*, **407**, 420
- Salcedo A. N., Maller A. H., Berlind A. A., Sinha M., McBride C. K., Behroozi P. S., Wechsler R. H., Weinberg D. H., 2018, *MNRAS*, **475**, 4411
- Schaap W. E., van de Weygaert R., 2000, *A&A*, **363**, L29
- Schawinski K., et al., 2014, *MNRAS*, **440**, 889
- Shandarin S. F., Zeldovich Y. B., 1989, *Reviews of Modern Physics*, **61**, 185
- Sousbie T., 2011, *MNRAS*, **414**, 350
- Sousbie T., 2013, *DisPerSE: Discrete Persistent Structures Extractor*, *Astrophysics Source Code Library*, record ascl:1302.015 (ascl:1302.015)
- Sousbie T., Pichon C., Kawahara H., 2011, *MNRAS*, **414**, 384
- Springel V., 2010, *MNRAS*, **401**, 791
- Springel V., White S. D. M., Tormen G., Kauffmann G., 2001, *MNRAS*, **328**, 726
- Springel V., et al., 2018, *MNRAS*, **475**, 676
- Tempel E., Libeskind N. I., 2013, *ApJ*, **775**, L42
- Tempel E., Stoica R. S., Saar E., 2013, *MNRAS*, **428**, 1827
- Trujillo I., Carretero C., Patiri S. G., 2006, *ApJ*, **640**, L111
- Tukey J. W., 1958, *The Annals of Mathematical Statistics*, **29**, 614
- Vogelsberger M., et al., 2014a, *MNRAS*, **444**, 1518

- Vogelsberger M., et al., 2014b, *Nature*, **509**, 177
- Vulcani B., Poggianti B. M., Fritz J., Fasano G., Moretti A., Calvi R., Paccagnella A., 2015, *ApJ*, **798**, 52
- Wang P., Libeskind N. I., Tempel E., Pawlowski M. S., Kang X., Guo Q., 2020, *ApJ*, **900**, 129
- Weinmann S. M., van den Bosch F. C., Yang X., Mo H. J., 2006, *MNRAS*, **366**, 2
- White S. D. M., 1994, Formation and Evolution of Galaxies: Les Houches Lectures ([arXiv:astro-ph/9410043](https://arxiv.org/abs/astro-ph/9410043))
- White S. D. M., Rees M. J., 1978, *MNRAS*, **183**, 341
- Yuan S., Hadzhiyska B., Bose S., Eisenstein D. J., 2022, *MNRAS*, **512**, 5793
- Zehavi I., et al., 2011, *ApJ*, **736**, 59
- Zehavi I., Contreras S., Padilla N., Smith N. J., Baugh C. M., Norberg P., 2018, *ApJ*, **853**, 84
- Zel'dovich Y. B., 1970, *A&A*, **5**, 84
- Zhang Y., Yang X., Wang H., Wang L., Luo W., Mo H. J., van den Bosch F. C., 2015, *ApJ*, **798**, 17
- Zheng Z., Weinberg D. H., 2007, *ApJ*, **659**, 1
- Zheng Z., et al., 2005, *ApJ*, **633**, 791
- de Lapparent V., Geller M. J., Huchra J. P., 1986, *ApJ*, **302**, L1
- van de Weygaert R., Schaap W., 2009, in Martínez V. J., Saar E., Martínez-González E., Pons-Bordería M. J., eds, , Vol. 665, Data Analysis in Cosmology. pp 291–413, [doi:10.1007/978-3-540-44767-2_11](https://doi.org/10.1007/978-3-540-44767-2_11)
- van den Bosch F. C., Yang X., Mo H. J., 2003, *MNRAS*, **340**, 771

This paper has been typeset from a $\text{\TeX}/\text{\LaTeX}$ file prepared by the author.